Effect of oxygen on short-range order in the Ba1-xBixF2+x solid solution

Malika El Omari, Mohamed El Omari, A. Abaouz, A. Zahouane, T. V. Serov, E. N. Dombrovski, E. I. Ardashnikova, N. G. Haban, V. A. Dolgikh, Jean Sénégas

Effect of oxygen on short-range order in the $Ba_{1-x}Bi_xF_{2+x}$ solid solution

Malika El Omari[a], Mohamed El Omari[a,*], A. Abaouz[a], A. Zahouane[a], T.V. Serov[b], E.N. Dombrovski[b], E.1. Ardashnikova[b], N.G. Haban[c], V.A. Dolgikh[b], J. Sénégas[d]

[a] *Department of Chemistry, Faculty of Science, Moulay Ismail University, 50000 Meknès, Morocco*
[b] *Chemistry Faculty, Lomonosov Moscow State University, Vorobjovy Gory, Moscow 119899, Russia*
[c] *Lomonosov State Academy of Fine Chemical Technology, pr. Vernadskogo 86, Moscow 117571, Russia*
[d] *Institut de Chimie de la Matière Condensée de Bordeaux (ICMCB), 87 Avenue Docteur Albert Schweitzer, 33608 Pessac Cedex, France*

Abstract

Various compositions within the range of the fluorite-type solid solution in the $BaF_2-BiF_3-BiO_{1.5}$ system are investigated by impedance spectroscopy. This study is carried out along two lines of compositions: δ_1, corresponding to the $Ba_{1-2z/3}Bi_{2z/3}F_{2+4z/3}O_z$ solid solution, where z is the oxygen rate; and δ_2, corresponding to the $Ba_{1-x}Bi_xF_{2+x-0.30}O_{0.15}$ solid solution, where x is the bismuth rate. An approach to the nature of the fluorine–oxygen order is proposed which derives from the clustering process in the $Ba_{1-x}Bi_xF_{2+x}$ fluoride solid solution.

Keywords: Electrical properties; F^- ion conductors; Fluorite-type structure; Characterization methods; Impedance spectroscopy; Clustering process

1. Introduction

Various clustering processes were proposed within the anion-excess $M_{1-x}^{2+}M'^{2+\alpha}_{x}F_{2+\alpha x}$ ($\alpha = 1$, 2) solid solutions with the fluorite-type structure [1–5]. They depend on the nature of the cationic couples (M, M′) present in the solid solution. For instance, the short-range order in the $Ba_{1-x}Bi_xF_{2+x}$ solid solution consists of a progressive transformation, on increasing x, of 4:4:3:0 clusters into 8:12:1:0 cuboctahedral clusters [6]. On the contrary, $A_{0.5(1-x)}Bi_{0.5(1+x)}F_{2+x}$ (A = Na, K) solid solutions only include cuboctahedral clusters [7]. The clustering processes also depend on the presence of mixed anions. A hypothesis is given in Ref. [8], which assumes that the addition of oxygen atoms, in Bi_2O_3 form, to $A_{0.5(1-x)}Bi_{0.5(1+x)}F_{2+x}$ ($0.60 \le x \le 0.70$ for A = Na and $0.50 \le x \le 0.70$ for A = K), induces a transformation of the cuboctahedral clusters into entirely fluorinated cubic entities and mixed cubic ones containing two oxygen and six fluorine atoms.

In order to complete the above studies, we have investigated in the present work the influence of the presence of oxygen on the clustering process in $Ba_{1-x}Bi_xF_{2+x}$ solid solution, with the aim to study the electrical properties of two series compositions of the fluorite-type structure solid solution, δ_1, corresponding

* Corresponding author.
E-mail address: melomari@fsmek.ac.ma (M. El Omari).

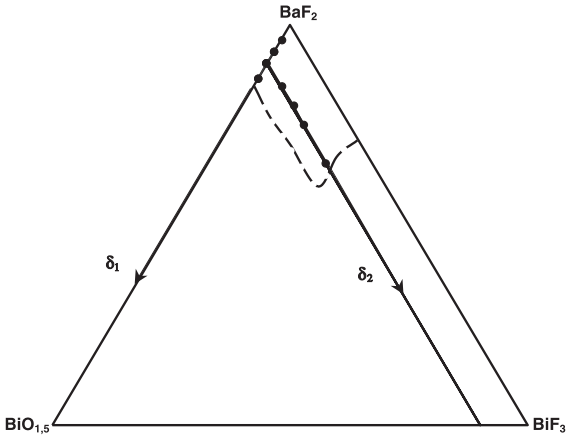

Fig. 1. Range of the oxy–fluoride solid solution with the fluorite-type structure in the BaF_2–BiF_3–$BiO_{1.5}$ system.

to $Ba_{1-2z/3}Bi_{2z/3}F_{2+4z/3}O_z$, and δ_2, corresponding to $Ba_{1-x}Bi_xF_{2+x-0.30}F_{0.15}$, where x and z are related to the bismuth and oxygen rate, respectively (Fig. 1).

2. Experimental

2.1. Synthesis

The starting materials were high-purity (>99.9%) barium and bismuth fluoride and bismuth oxide. BaF_2 was dried under vacuum (≈ 1 Pa) at 423 K for 2 h prior to the synthesis experiments, and the Bi_2O_3 oxide was annealed at 1073 K for 12 h to remove traces of water, hydroxides and carbonates. BiF_3 was prepared from $Bi(OH)_3$ by reaction with aqueous HF (40%), and the obtained precipitate was heated at 623 K for 3 h under a flow of anhydrous HF. Ready to use starting materials were kept in a dry box.

The mixed powders of BaF_2, BiF_3 and Bi_2O_3, taken in appropriate ratios, were ground in the dry box and introduced into copper tubes. This metal proved to be a satisfying container in previous experiments. After degassing under vacuum at 473 K for 2 h and filling with dry argon, the copper tubes were sealed, heated at 873 ± 10 K for 12 h and finally quenched in icy water. X-ray powder diffraction patterns were recorded with a Guinier camera FR-552 (Cu-Kα1 radiation) using germanium as an internal standard. All samples were single-phase, with a fluorite-type structure and a unit-cell parameter ranging from $a = 6.023(2)$ to $6.200(2)$ Å.

2.2. Electrical conductivity measurements

Conductivity measurements have been carried out on powder samples pressed to form pellets having a thickness of ≈ 1 mm and a diameter of ≈ 8 mm, sintered under the same operating conditions as for the synthesis. Compactness is close to 90% for all samples. A gold electrode was deposited on both sides of the pellet by vacuum evaporation. The Au//sample//Au devices were placed in a quartz measurement cell, degassed at 473 K for 2 h and filled with dry argon to avoid eventual hydrolysis. Electrical properties were determined by complex impedance method [9] using a Solartron 1260 frequency response analyser. The frequency range was between 10^{-1} and 10^6 Hz over the thermal interval from 300 to 700 K in several temperature cycles. For each temperature measurement, the sample was kept at the desired temperature during 30 min and was then heated automatically by steps of 10°.

3. Results

3.1. Impedance hodographs

Some complex impedance diagrams of $Z''(\Omega)$ as a function of Z' (Ω), i.e. the so-called Cole–Cole diagrams [10], are given in Fig. 2 for the $Ba_{1-x}Bi_xO_{0.15}F_{2+x-0.30}$ solid solution at $T = 408$, 418, 428 and 438 K for $x = 0.10$, $T = 403$, 413, 423 and 428 K for $x = 0.25$ and $T = 473$, 483, 493 and 503 K for $x = 0.35$. Each curve shows at high frequency a semicircular part, which is characteristic of volume properties, whereas the experimental points at low frequency are located on a straight line, which is specific of electrode polarization phenomena. With increasing temperature, the intercept of this linear part with the real axis is shifted to lower R-values. The bulk ohmic resistance relative to each composition at a given temperature can be calculated from the intercept on the real axis of the zero phase angle extrapolation of the highest-frequency curve ($Z^* = Z' - jZ'' = R\exp(j\varphi\omega)$). As a matter of fact, the

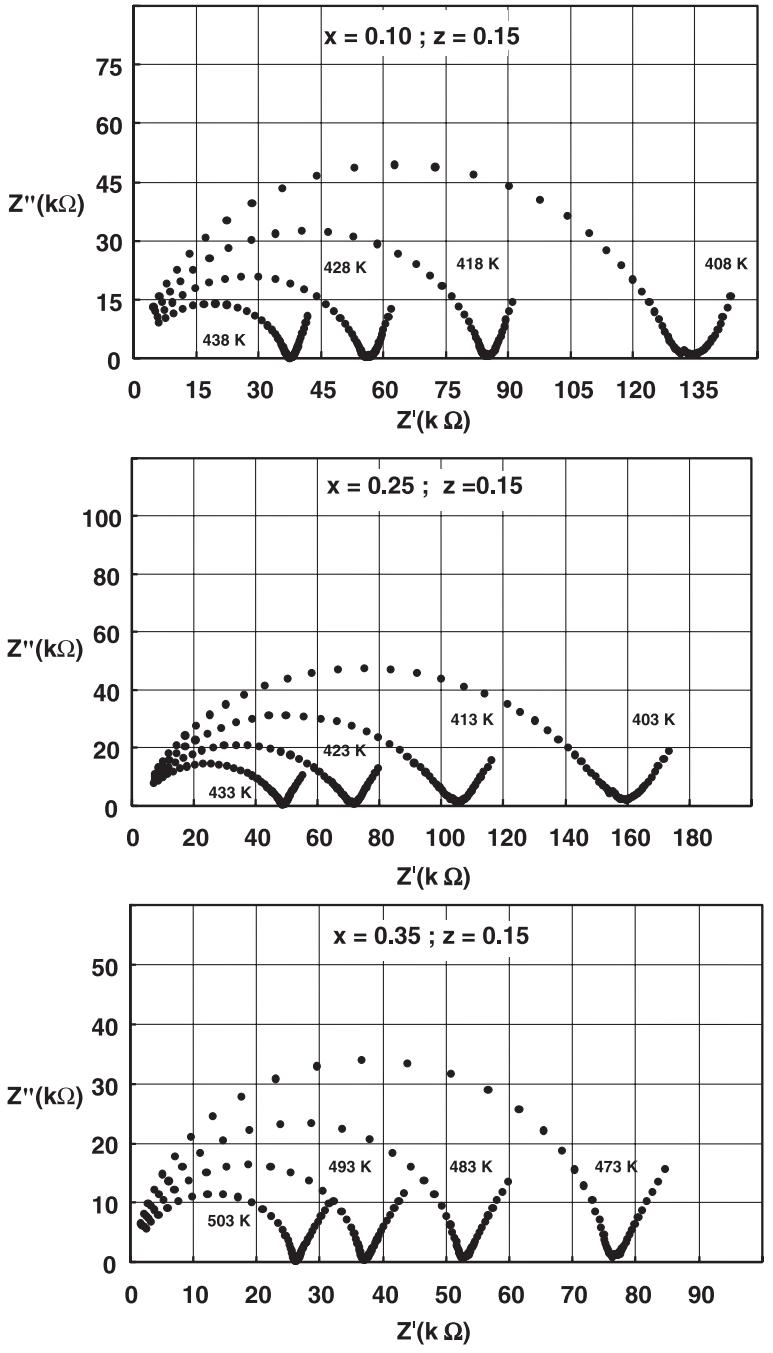

Fig. 2. Impedance spectra relative to some samples of the $Ba_{1-x}Bi_xF_{2+x-0.30}O_{0.15}$ solid solution.

samples studied here are ceramic compounds and they obviously involve a bulk ionic conductivity and/or a grain boundary ionic conductivity. To separate the contribution of the two components, it is necessary to simulate the experimental spectra on the basis of an equivalent electric circuit.

3.2. Equivalent electric circuits

An equivalent circuit that contains two, three or more elements may be modified in various combinations but still yields the same overall ac response. This leads to the notion that there is no unique equivalent circuit for a particular system. Thus, the problem is to determine which equivalent circuit should be used for the analysis and interpretation of the electrical behaviour of a system. Usually, the equivalent circuit is based on the following:

- intuition as to what kind of impedances are expected to be present in the studied system and whether they are connected in series or parallel,
- examination of the experimental data to conclude whether the response is consistent with the proposed circuit,
- inspection of R and C values obtained in order to check if they are realistic and their temperature dependence, if any, is reasonable.

An equivalent circuit widely used to represent bulk and grain boundary phenomena in polycrystalline materials consists of two parallel R_bC_b and $R_{gb}C_{gb}$ elements connected in series [11]. The determination of different electrical components of the circuit is best achieved using a combination of impedance and electrical modulus formalisms, since each parallel RC element gives rise to a semicircle in the complex plan, Z'' vs. Z', M'' vs. M', or a Debye peak in the plots of the imaginary functions, Z''; M'' vs. $\log(f)$ [12].

The response in the Z^* plane for a single parallel RC element has the form of a semicircular arc which passes through the origin and whose low frequency intercept on the real axis corresponds to the resistance R of the element. In practice, semicircles associated with bulk relaxation processes in the Z^* plots of many conducting materials are found to be non-ideal. Depressed semicircles are obtained whose centres are displaced below the real axis. There are two main reasons for such a non-ideal behaviour:

(i) the presence of a distribution in relaxation times within the bulk response [13],

(ii) a distortion due to other relaxations, i.e. grain boundary relaxations, whose time constants are within two orders of magnitude of that of the bulk [12,14] (same order of magnitude).

The Z^* hodographs obtained for each sample of the $Ba_{1-x}Bi_{x.15}F_{2+x-2y}O_z$ solid solution are consistent with the equivalent electric circuit shown in Fig. 3. The semicircles of the $Z''=f(Z')$ curve which appear successively at decreasing frequency (Fig. 2) are associated with relaxation processes characteristic of intragranular R_bC_b and intergranular $R_{gb}C_{gb}$ resistivity, respectively. The polarization phenomena at the electrode–electrolyte interface are expressed in the capacitance element C_3.

For a given temperature, the values of R_b and R_{gb} parameters have been, at first, estimated from the experimental spectra at low frequency intercepts of each semicircle with the real axis. The values of C_b and C_{gb} have been estimated from experimental points corresponding for each relaxation process to the frequency ω_{max} of the Z'' maximum ($\omega=2\pi f$=angular frequency). In-deed, ω_{max}, R and C for a parallel RC element are related by the following relationship: $\omega_{max}RC=1$.

The dispersive properties of different relaxation processes have been taken into account in the simulation of impedance spectra by writing the complex capacitance C_i of each R_iC_i element as [15]:

$$C_i = B_i(j\omega,)^{n_i} \quad (0 < n_i < 1)$$

(B is the real capacitance)

A fitting approach is calculated for each temperature by complex non-linear least squares fitting of

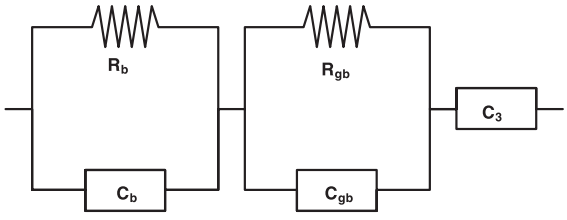

Fig. 3. Equivalent electric circuit.

both the real and the imaginary part of $Z^*(\omega)$. The program used for this work is LEVEM version 7.0 [16]. Typical fitting results of $Ba_{0.90}Bi_{0.10}F_{1.80}O_{0.15}$ sample at $T=363$ and 423 K, and $Ba_{0.80}Bi_{0.20}F_{1.90}O_{0.15}$ sample at $T=353$ and 383 K are shown, for instance, in Fig. 4a and b, respectively, where the relative residuals are defined by the relationship [17]:

$$\Delta_{re} = (Z'_{measured} - Z'_{calculated})/Z'_{measured}, \text{ and}$$
$$\Delta_{im} = (Z''_{measured} - Z''_{calculated})/Z''_{measured}$$

An optimum fit is obtained as the relative residuals are spread randomly around the frequency axis; the relative errors are less than 8% in the measurement frequency range (Fig. 4a and b), in agreement with the experimental error. Therefore, an excellent agreement between experimental and theoretical calculation data has been obtained in a wide frequency range, confirming the validity of the proposed equivalent electric circuit.

3.3. Modulus hodographs

Electrical data were also analysed using the complex modulus formalism, $M^* = 1/\varepsilon^* = j(\omega C_0)Z^*$, where C_0 is the vacuum capacitance of the empty measuring cell, in order to determine the conductivity relaxation parameters. Considering an equivalent electric circuit composed of two parallel *RC* elements associated in series, the modulus plot gives emphasis on the element with the smallest capacitance, whereas the impedance plot highlights that with the largest resistance. Consequently, the M^* formalism can discriminate against grain boundary phenomena, electrode polarization and other interfacial effects in solid electrolytes [11,12]. Frequency dependence of the normalized imaginary part of M^*, M''/M''_{max}, is given in Fig. 5, for some samples of the $Ba_{1-x}Bi_xF_{2-x-0.30}O_{0.15}$ solid solution at $T=323$, 343, 363 and 383 K for $x=0.10$, at $T=303$, 323, 343 and 363 K for $x=0.20$ and at $T=393$, 413, 433 and 453 K for $x=0.35$. Whatever the temperature, a single maximum is observed which is characteristic of the bulk properties of the sample. With increasing temperature, the modulus peak maximum shifts to higher frequencies. The frequency range where the peak occurs is indicative of the transition at decreasing frequency from short-range to long-range mobility and is defined by the relation $\omega\tau_\sigma = 1$, where τ_σ is the most probable ion relaxation time [13,18]. The M''/M''_{max} curves are non-symmetric, in agreement with the non-exponential behaviour of the electrical function that is well described by the empirical stretched exponential Kohlrausch function $\varphi(t) = \exp[-(t/\omega\tau_\sigma)^\beta]$ $(0<\beta<1)$ [13,19,20]. The full width at half maximum (FWHM) of the M''/M''_{max} spectrum is wider than the breadth of a Debye peak (1.14 decades) and results in a β value ($\beta = 1.14/\text{FWHM}$) less than the one for the Kohlrausch parameter. The β values obtained for each composition of the $Ba_{1-x}Bi_xF_{2-x-0.30}O_{0.15}$ solid solution are temperature independent (Table 1). The β parameter can be interpreted as representative of a distribution of relaxation times generating the dispersive properties of the studied materials [13]. This distribution could then imply the presence of different types of F^- ions in these materials.

An excellent agreement between the experimental and calculated data values has also been obtained for the modulus formalism (Fig. 4a and b), which is another confirmation of the validity of the equivalent electric circuit proposed to explain the electrical properties in these materials.

3.4. Electrical parameters

The bulk ohmic resistance of each studied composition of the $Ba_{1-x}Bi_xF_{2+x-2z}O_z$ solid solution, relative to each experimental temperature, is determined by simulation of the electrical data. The temperature dependence of conductivity between 300 and 675 K is plotted in Fig. 6 as $\log \sigma T$ vs. $1000/T$ for the $Ba_{1-2z/3}Bi_{2z/3}F_{2-4z/3}O_z$ (δ_1) and $Ba_{1-x}Bi_xF_{2+x-0.30}O_{0.15}$ (δ_2) solid solutions. The temperature dependence of the jump frequency of mobile ions, f_p, corresponding to the relaxation frequency relative to M''_{max}, is also given in Fig. 6 (right part). For each composition, both observed lines are quasi-parallel and typical of an Arrhenius behaviour $\sigma T = \sigma_0 \exp[\Delta E_\sigma/kT]$ and $f_p = f_0 \exp[\Delta E_f/kT]$ with a fitting coefficient $R^2>0.98$. The ΔE_f activation energy determined for each composition from the modulus spectra is very close to the ΔE_σ activation energy issued from the impedance spectra (Table 2). These results suggest that the F^- ion transport in the $Ba_{1-x}Bi_xF_{2+x-2z}O_z$ oxide–fluoride solid solution is probably due to a hopping mechanism [21].

The composition dependence of conductivity, $\log\sigma = f(x)$, at $T = 473$ K and activation energy, ΔE_σ, determined for both $Ba_{1-2z/3}Bi_{2z/3}F_{2-4z/3}O_z$ and $Ba_{1-x}Bi_xF_{2+x-0.30}O_{0.15}$ solid solutions are plotted in Fig. 7a and b, respectively. As a comparison, the composition dependence of the electrical parameters

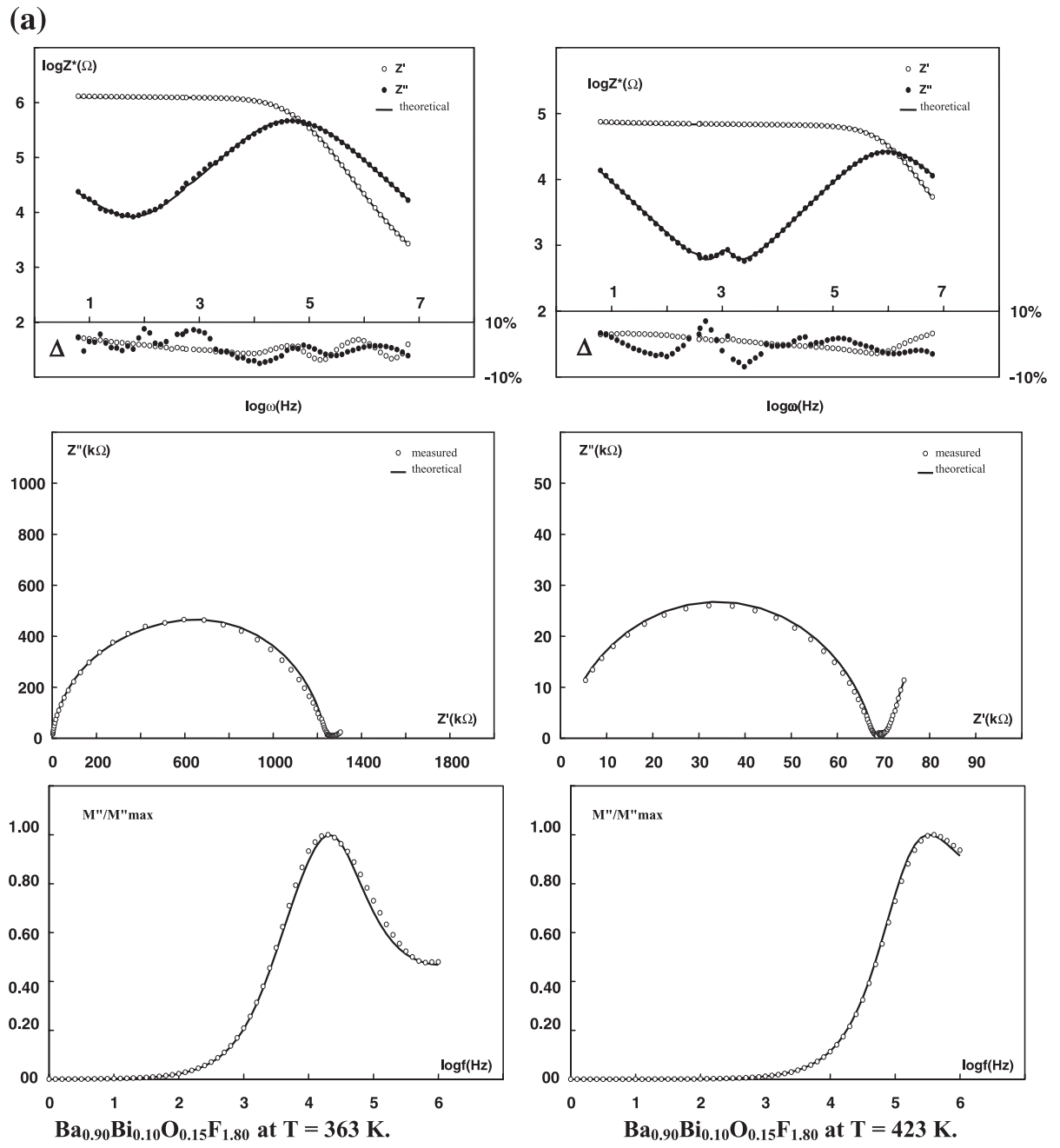

Fig. 4. Experimental and calculated impedance and normalized modulus data for (a) $Ba_{0.90}Bi_{0.10}F_{1.80}O_{0.15}$ at $T = 363$ and 423 K, and (b) $Ba_{0.80}Bi_{0.20}F_{1.90}O_{0.15}$ at $T = 353$ and 383 K.

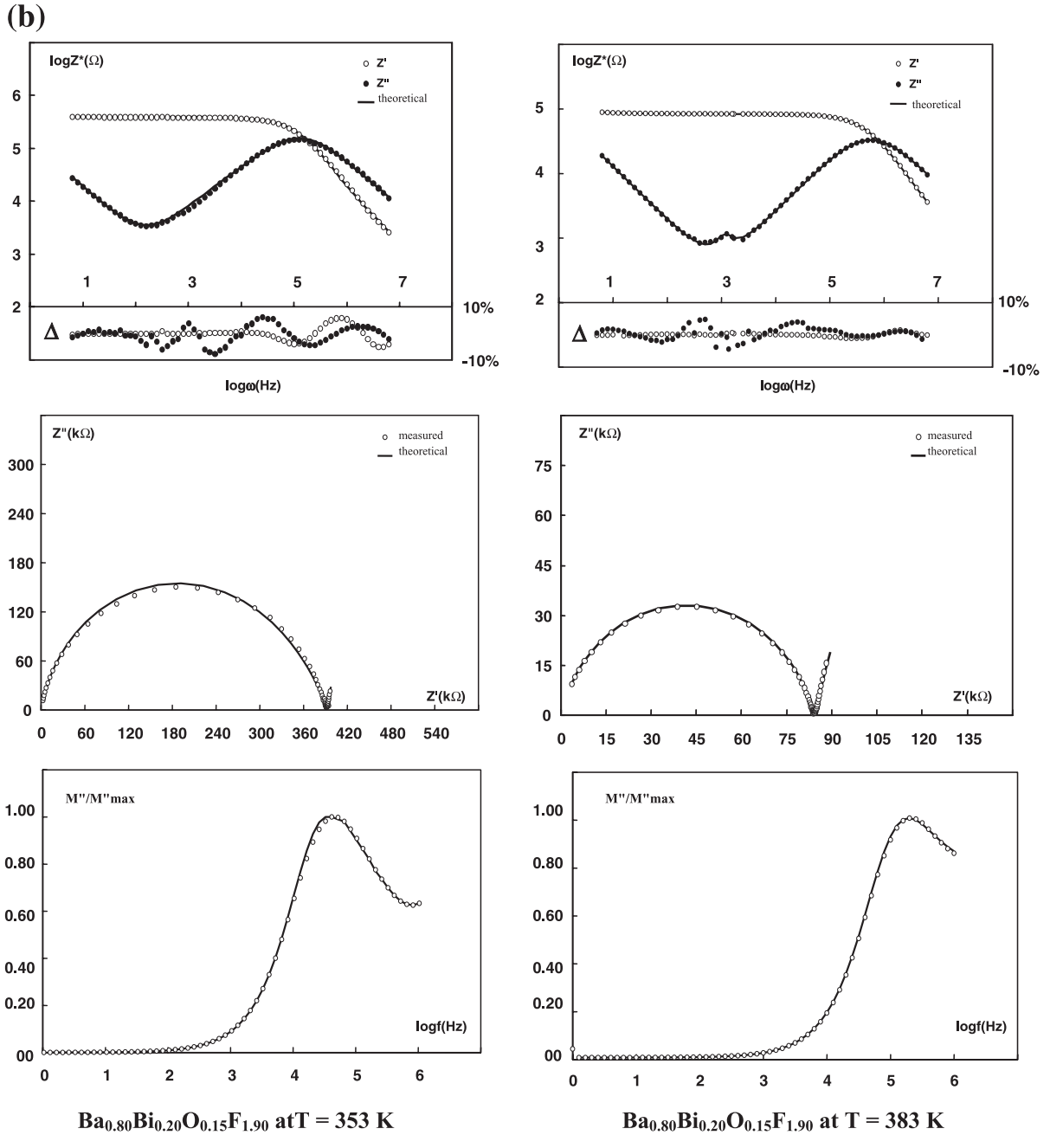

Fig. 4 (*continued*).

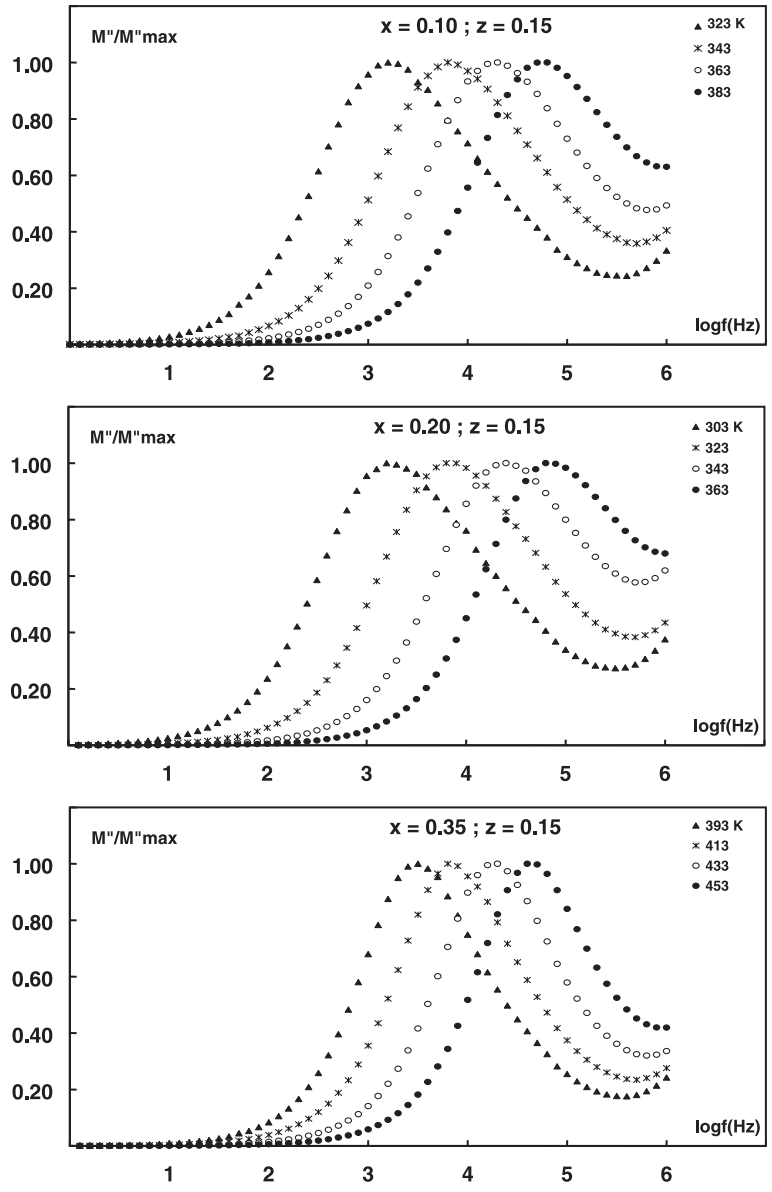

Fig. 5. Plots of normalized modulus ($M''/M''_{max.}$) vs. log(f) for some compositions of the $Ba_{1-x}Bi_xF_{2+x-0.30}O_{0.15}$ solid solution at various temperatures.

of $Ba_{1-x}Bi_xF_{2+x}$ fluoride solid solution [6] is also reported in Fig. 7b.

In the $Ba_{1-2z/3}Bi_{2z/3}F_{2-4z/3}O_z$ solid solution, which shows an anionic deficit and corresponds to the formal substitution reaction: $Ba^{2+} + 2F^- \rightarrow Bi^{3+} + O^{2-}$ (with the formation of one anionic vacancy [V]), the ionic conductivity increases and the activation energy decreases regularly with growing oxygen rate. These results explain that the presence of oxygen anion in these materials involves an improvement of the electrical properties. On the contrary, in the $Ba_{1-x}Bi_xF_{2+x-0.30}O_{0.15}$ solid solution, which is anionic

Table 1
Kohlrausch parameter β for some compositions of the $Ba_{1-x}Bi_xF_{2+x-0.30}O_{0.15}$ solid solution

x	β
0.10	0.54 ± 0.02
0.15	0.55 ± 0.02
0.20	0.53 ± 0.02
0.25	0.53 ± 0.02
0.35	0.70 ± 0.02

deficient for $x<0.15$ and anionic excessive for $x>0.15$ and corresponds to the substitution reaction: $Ba^{2+} \rightarrow Bi^{3+} + F^-$ (with $Ba_{0.85}Bi_{0.15}F_{1.85}O_{0.15}$ as starting composition), two domains of composition exist. On the anionic deficient side, the substitution reaction implies the filling of a vacancy, while on the anion excessive one, it involves the formation of an interstitial F^- ion. For $x<0.20$, the electrical conductivity increases regularly with increasing x, but a strong lowering is observed for $x>0.20$. So, the composition $x \approx 0.20$ presents the best electrical performances in the $Ba_{1-x}Bi_xF_{2+x-0.30}O_{0.15}$ solid solution. It appears that the evolution of the electrical properties as a function of composition of this oxy–fluoride solid solution and those of the $Ba_{1-x}Bi_xF_{2+x}$ fluoride solid solution is very similar, except that the composition x_{max} corresponding to a conductivity maximum associated with a minimum activation energy obtained for the $Ba_{1-x}Bi_xF_{2+x-0.30}O_{0.15}$ solid solution (x_{max} = 0.20) is lower than for $Ba_{1-x}Bi_xF_{2+x}$ (x_{max} =0.35) [6].

3.5. Proposal of a clustering process

3.5.1. In the $Ba_{1-x}Bi_xF_{2+x-0.30}O_{0.15}$ solid solution

The electrical properties of the $Ba_{1-x}Bi_xF_{2+x-0.30}O_{0.15}$ solid solution for $x \leq 0.20$ are very close of those of the $Ba_{1-x}Bi_xF_{2+x}$ one, where a progressive transformation of 4:4:3:0 clusters into 8:12:1:0 cuboctahedral entities with increasing x takes place [6]. The 4:4:3:0 cluster is formed by four vacancies, four F'-type interstitial fluoride ions, three F''-type interstitial fluoride ions and zero F'''-type interstitial fluoride ions. The presence of this cluster in a solid solution is favourable for transport properties implying the F' and F'' ions, in contrary to the 8:12:1:0 cuboctahedral entity (8 vacancies, 12 F'-type interstitial fluoride ions, 1 F''-type interstitial fluoride ion and 0 F'''-type interstitial fluoride ions), where the motion of interstitial fluorides only involves a short-range distance. The increase of conductivity for $x<0.35$ was explained by the high number of 4:4:3:0 clusters. On the contrary, for $x>0.35$, the number of 8:12:1:0 entities becomes more and more dominant, which explains the conductivity fall [6]. This result allows to deduce that for two compositions of the above solid solutions having the same Bi^{3+} rate, the number of mobile ions is practically identical. This result proves that the clustering process in the $Ba_{1-x}Bi_xF_{2+x-0.30}O_{0.15}$ and $Ba_{1-x}Bi_xF_{2+x}$ solid solutions is identical. The oxygen ions preferentially substitute the fluoride ions in normal position in the $Ba_{1-x}Bi_xF_{2+x}$ solid solution, introducing more vacancies in the oxy–fluoride materials. As is the case in the $Ba_{1-x}Bi_xF_{2+x}$ solid solution, the conductivity falls in the $Ba_{1-x}Bi_xF_{2+x-0.30}O_{0.15}$ solid solution for $x>0.20$, a result that may be explained by the presence of cuboctahedral clusters. This result allows to deduce that the progressive transformation of the 4:4:3:0 clusters into 8:12:1:0 ones is favoured by the presence of a high number of vacancies.

$Ba_{0.65}Bi_{0.35}F_{2.05}O_{0.15}$ corresponds to the upper limit of the $Ba_{1-x}Bi_xF_{2+x-0.30}O_{0.15}$ solid solution along the δ_2 line (Fig. 1), whence the higher value of the β Kohlrausch parameter (0.70(2)) in comparison to those of the other studied compositions (β =0.54(2), and composition independent). This result suggests that the upper limit of the solid solution only contains cuboctahedral clusters, whereas the other studied compositions involve a mixture of 4:4:3:0 and 8:12:1:0 clusters.

3.5.2. In the $Ba_{1-2z/3}Bi_{2z/3}F_{2-4z/3}O_z$ solid solution

The experimental results for both the i and j compositions located along the two different lines δ_1 and δ_2 (Fig. 1) and having a close Bi^{3+} rate show the same conductivity and activation energy (Fig. 7a and b). It appears that the clustering process for $Ba_{1-2z/3}Bi_{2z/3}F_{2-4z/3}O_z$ solid solution corresponds to the formation of 4:4:3:0 clusters too. To maintain the total anion-deficient composition, such clusters must coexist with more anionic vacancies. The absence of any break in the electrical properties dependence along the δ_1 line when crossing the stoichiometry line (x = 0.15; Fig. 7b) serves as another proof of the same clustering process.

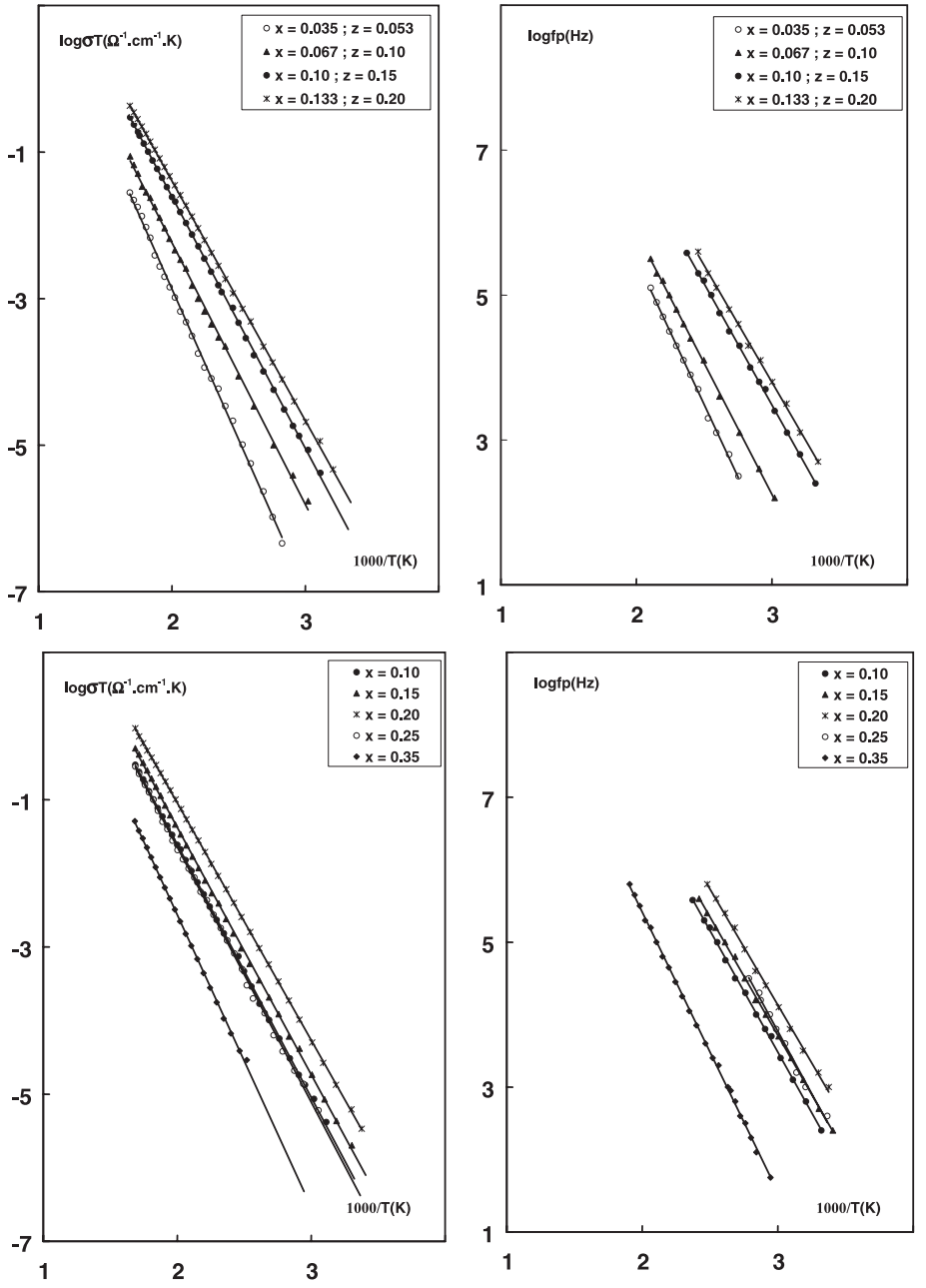

Fig. 6. Temperature dependence of $\log(\sigma T)$ and $\log(f_p)$, where f_p is the $M''_{max.}$ peak frequency, relative to some compositions of the $Ba_{1-2z/3}Bi_{2z/3}F_{2-4z/3}O_z$ and $Ba_{1-x}Bi_xF_{2+x-0.30}O_{0.15}$ solid solutions.

One cannot exclude the presence of two phases (not yet shown by XRD) in the samples situated in the anionic-deficient domain (whole δ_1 line), because the presence of anion excess 4:4:3:0 clusters (four vacancies and seven interstitial anions) in this domain seems unusual. In this case, all the samples along

Table 2
Activation energy ΔE_σ stemmed from impedance spectra and ΔE_f stemmed from normalized modulus spectra relative to some compositions of the $Ba_{1-2z/3}Bi_{2z/3}F_{2-4z/3}O_z$ and $Ba_{1-x}Bi_xF_{2+x-0.30}O_{0.15}$ solid solutions

$Ba_{1-2z/3}Bi_{2z/3}F_{2-4z/3}O_z$			$Ba_{1-x}Bi_xF_{2+x-0.30}O_{0.15}$		
z	ΔE_σ (eV) ± 0.02	ΔE_f (eV) ± 0.02	x	ΔE_σ (eV) ± 0.02	ΔE_f (eV) ± 0.02
0.05	0.81	0.79	0.10	0.68	0.66
0.10	0.72	0.72	0.15	0.67	0.65
0.15	0.68	0.66	0.20	0.64	0.63
0.20	0.65	0.64	0.25	0.69	0.68
			0.35	0.79	0.77

the δ_1 line include more than 95% mass BaF_2 and can be considered as a mixture of two phases, one of the fluorite-type and the other of the Bi_2O_3 one. However, one should not forget that the electrical properties may then depend on the concentration of polarizable Bi^{3+} cations.

4. Conclusions

The bulk ohmic resistance of each studied composition of $Ba_{1-x}Bi_xF_{2+x-2z}O_z$ fluorite-type solid solution relative to each experimental temperature is determined by the simulation of electrical data band on an equivalent circuit widely used to represent bulk and grain boundary phenomena in polycrystalline materials.

The composition dependence of the electrical properties of the $Ba_{1-x}Bi_xF_{2+x-0.15}$ oxide–fluoride solid solution is analogous to that of the $Ba_{1-x}Bi_xF_{2+x}$

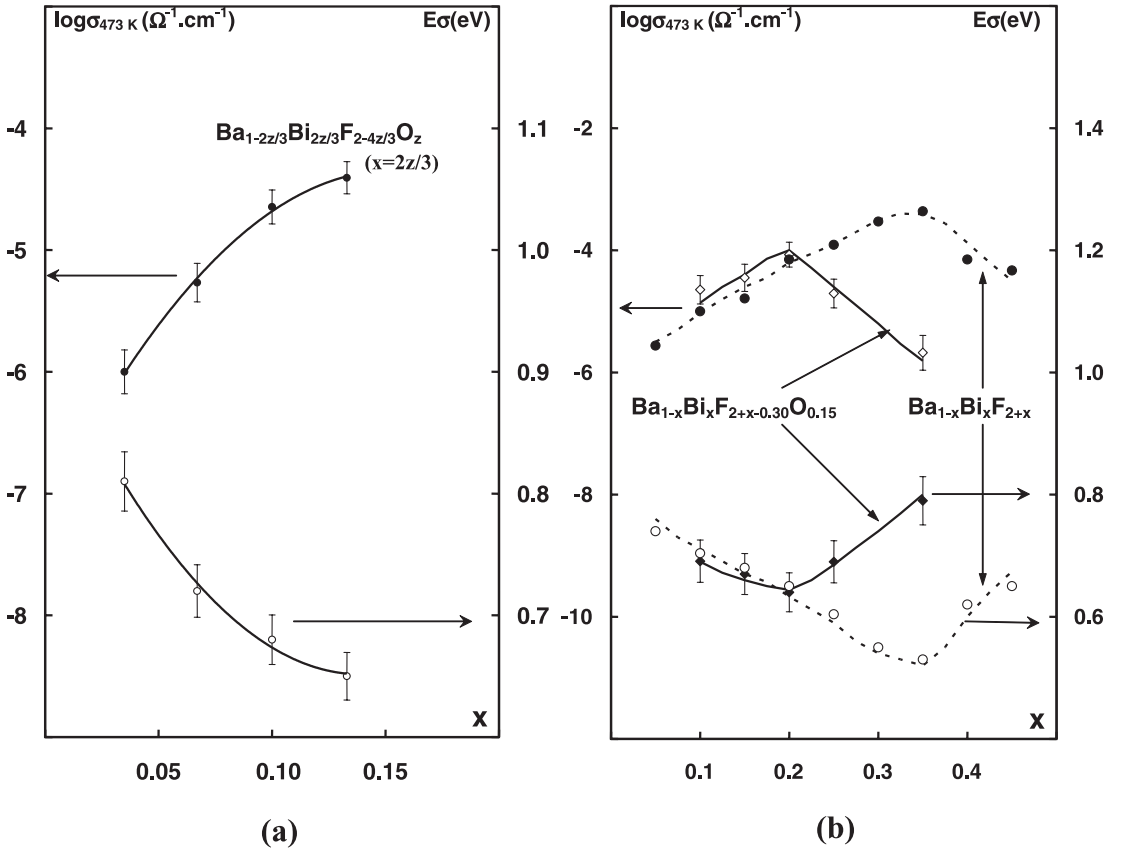

Fig. 7. Composition dependence of $\log(\sigma_{473\ K})$ and AE_σ for (a) the $Ba_{1-2z/3}Bi_{2z/3}F_{2-4z/3}O_z$ and (b) the $Ba_{1-x}Bi_xF_{2-x}$ and $Ba_{1-x}Bi_xF_{2+x-0.30}O_{0.15}$ solid solutions.

fluoride one. This result allows to deduce that for the same Bi^{3+} rate, the clustering process is identical in both solid solutions. It squares with a progressive transformation of 4:4:3:0 clusters into 8:12:1:0 cuboctahedral entities with increasing x.

Acknowledgements

The authors are grateful to the Russian Foundation for Basic Research (grant No 02-03-32847) and Russian Ministry of Higher Education (grant No 2000 T00-9.4-1992) for their support.

References

[1] A.M. Golubev, A.K. Ivanov-Shitz, V.I. Simonov, B.P. Sobolev, N.I. Sorokin, P.P Fedorov, Solid State Ionics 37 (1990) 115.

[2] J.-M. Réau, P. Hagenmuller, Bull. Electrochem. 11 (1995) 34.

[3] J.-M. Réau, X.Y. Jun, J. Sénégas, P. Hagenmuller, Solid State Ionics 78 (1995) 315.

[4] M. El Omari, J.L. Soubeyroux, J.-M. Réau, J. Sénégas, Solid State Ionics 130 (2000) 133.

[5] B.P. Sobolev, The Rare Earth Trifluorides, Part 2, Barcelona, 2001, 460 pp.

[6] S.K. Soo, J. Sénégas, J.-M Réau, M. Wahbi, P. Hagenmuller, J. Solid State Chem. 97 (1992) 212.

[7] C. Chartier, J. Grannec, J.-M. Reau, J. Portier, P. Hagenmuller, Mater. Res. Bull. 16 (1981) 1159.

[8] M. El Omari, J.-M. Réau, J. Sénégas, T.V. Serov, E.I. Ardashnikova, V.A. Dolgikh, J. Fluorine Chem. 113 (2002) 37.

[9] F. Bauerle, J. Phys. Chem. Solids 30 (1969) 2657.

[10] D.P. Almond, A.R. West, Solid State Ionics 11 (1983) 57.

[11] I.M. Hodge, M.D. Ingram, A.R. West, J. Electroanal. Chem. 74 (1976) 125.

[12] D.C. Sinclair, Bol. Soc. Esp. Ceram. Vidr. 34 (1995) 55.

[13] F.S. Howell, R.A. Bose, P.B. Macedo, C.T. Moynihan, J. Phys. Chem. 78 (1974) 639.

[14] D. Ming, J.-M. Réau, J. Ravez, G. Joo, P. Hagenmuller, J. Solid State Chem. 116 (1995) 185.

[15] A.K. Jonscher, Dielectric Relaxation in Solids, Chelsea Dielectric Press, 1983.

[16] J. Ross Macdonald, LEVM program, version 7.0 (1997).

[17] J. Ross Macdonald, J. Electroanal. Chem. 378 (1994) 17.

[18] H.K. Patel, S.W. Martin, Phys. Rev. B45 (1992) 10292.

[19] G. Williams, D.C. Watts, Trans. Faraday Soc. 23 (1970) 625.

[20] K.L. Ngai, S.W. Martin, Phys. Rev. B40 (1989) 10550.

[21] B.V.R. Chowdari, R. Gopalakrishnan, Solid State Ionics 23 (1987) 225.